Proceedings of Global Power and Propulsion Society
ISSN-Nr: 2504-4400
GPPS Hong Kong 2023
October 17-19, 2023
www.gpps.global

GPPS-TC-2023-0080

Deriving Sensitivities of Distributed Propeller Propulsion in Overwing Configuration by using DoE in CFD Simulations

Bastian Kirsch, Jens Friedrichs
Cluster of Excellence SE^{2}A - Sustainable and Energy-Efficient Aviation
Institute of Jet Propulsion and Turbomachinery, Technische Universität Braunschweig
b.kirsch@ifas.tu-braunschweig.de
Braunschweig, Germany

ABSTRACT

In this publication the interaction of propeller and wing of a short haul aircraft concept with distributed propeller propulsion in an over-wing configuration at cruise conditions is investigated. The numerical studies are performed in the CFD solver TAU of the German Aerospace Center using the Actuator Disk together with a wing segment with constant chord length. All calculations are performed in trimmed condition, i.e. with constant lift and drag coefficients. The resulting propeller power is used as a comparative variable. In order to quantify the influences of the position in chord direction, distance to the wing surface, installation angle, propeller diameter as well as distance between the propellers, a design of experiments approach with face centered central composite design is used. The resulting regression model is shown and analyzed. The procedure is carried out with two different propeller designs. In the first run, a propeller designed for a conventional aircraft with one propeller per half span is used. In the second run, a propeller designed for a distributed propulsion concept facing lower loads is used. The changes in the regression models are shown and compared. It hast been shown that the chord position has a significant influence on the performance of the propeller. The lowest power is reached when the propeller is positioned above the trailing edge of the wing. In addition, there is a dependence on the installation angle, which roughly follows the surface curvature of the airfoil. For the distance to the top of the wing, only a negligible effect on the propeller performance was found. For a positioning above the trailing edge, the propeller diameter and the spanwise distance between the propellers were found to be dominant parameters. Even when using a different propeller design, the linear dependence remains. For both propellers investigated, there is a similar optimal combination of diameter and spanwise distance with lowest power.

INTRODUCTION

Distributed propeller propulsion is seen as a possible technology for future short-haul aircraft. The interaction between the wing and the propeller is to be exploited in order to make the aircraft more efficient as an overall system. Various designs position the propellers in front of the leading edge of the wing (Deere et al. (2017), Keller (2021)) to exploit the effect of higher dynamic pressure in the slipstream of the propeller and to be able to dimension the wing smaller saving weight. The focus of recent research is diverse. The aerodynamic-propulsive coupling of propeller and wing is often investigated. Especially in the range of low flight speeds and high thrusts, which are characteristic for take off and climb segments, significant increases in lift can be achieved (Della Vecchia et al. (2018), Beckers et al. (2023)). In addition, noise emissions can be reduced through distribution and resulting reduction of power or thrust (Bernardini et al. (2020), Giraldo et al. (2022)). Finally, redundancy also increases safety. Since the drive trains are multiple, the one-engine-inoperative case is less demanding for the single units.

However, propellers positioned above the wing also offer advantages. All studies in which the propeller is positioned above the wing show drag reductions. Johnson and White (1983) investigated this experimentally with one propeller per half span in climb conditions ($C_L = 0.7$) and different wing configurations. The highest drag reduction of $\Delta C_D = -0.02$ compared to the isolated wing was found when the propeller is positioned at 20% of chord. For a positioning above the trailing edge a reduction of $\Delta C_D = -0.01$ was observed. No adverse effects on propeller efficiency compared to the isolated propeller performance were found. Cooper et al. (1992) also found significant drag savings with a simultaneous increase in the lift coefficient. A position study showed that positions close to the trailing edge provide higher lift coefficients ($\Delta C_L = 0.25$). The maximum drag reduction was found at 60% of chord with $\Delta C_D = -0.025$ compared to the isolated wing. The efficiency

of the propeller was not negatively affected. Veldhuis (2005) investigated the interactions between wing and propeller using a vortex lattice method. This confirmed the gains in lift and drag, but at the same time showed losses in the efficiency due to a clearly asymmetric loading of the propeller in overwing configurations. Investigations by Müller et al. (2014) with a channel wing could confirm the asymmetric load distribution of the propeller by means of CFD simulations. The investigations were performed at different flight Mach numbers where small drag reductions compared to the isolated wing of $\Delta C_D = -0.0025$ at Mach number of 0.6 and higher reductions $\Delta C_D = -0.006$ at Mach number of 0.4 were observed. It could also be determined that an overwing configuration is not competitive with a conventional configration due to the losses in propeller efficiency. The results for efficiency indicate that for a positioning at 40% of chord and a flight Mach number of 0.4 the propeller reaches about 92% of the efficiency of a classical tractor configuration. This value further decreases to 84% if the Mach number is increased to 0.6. Vries (2022) addressed in detail the issue of distributed propulsion in overwing configuration. Experimental and numerical studies were performed for this purpose. Three propeller positions as well as three distances to the wing upper surface were investigated in cruise conditions ($C_L \approx 0.5$). The highest lift increase of 15% compared to the isolated wing was reached at the most downstream position of 85% chord for the highest thrust setting. Again, decreased drag coefficients were observed due to reduced pressure drag. An overall increase in $\frac{L}{D}$ of up to 74% was reached for the highest thrust and still 8% for low thrust settings. Concerning the propeller efficiency, large impact of the relative chord position of the propeller was observed. While positions near the trailing edge achieved values of efficiency close to the isolated propeller, positions near the maximum thickness of the airfoil reduced the propeller efficiency between $10-13\%$. In studies carried out by the author (Kirsch and Friedrichs (2023)) it was found that propellers located close to the maximum thickness of the airfoil can increase lift by 9% and at the same time reduce drag by 45% compared to a conventional tractor configuration. However, the positioning of the propeller near the maximum thickness also forces the propeller to operate in the highest inflow speeds together with highly nonuniform inflow conditions decreasing the efficiency by more than 10%. Against this background, the question arises whether an application of distributed propulsion in overwing position brings advantages and what the sensitivities for this are. A direct comparison of different positions and installation situations can therefore only be provided from the perspective of the overall system under constant flight conditions (same lift and drag coefficient). This will show whether the integration effects (lower drag and increased lift) can outweigh the efficiency losses of the propeller.

METHODOLOGY

Numerical Solver

All investigations in this publication were performed with the TAU code of the German Aerospace Center (DLR). TAU solves the Navier-Stokes equations (RANS) with a second order finite volume method (Schwamborn et al. (2006)). The SST model of Menter et al. (2003) was used for turbulence modeling. Thus, all surfaces were calculated fully turbulent without laminar or transition effects.

Actuator Disk

In the investigations carried out, the propeller is modeled as an actuator disk and thus not fully resolved. For this purpose, the actuator disk integrated in TAU (Raichle et al. (2008)) is used, which is based on the blade element theory and frequently used in other publications e.g. Spinner et al. (2020), Keller (2021), Beckers et al. (2023). In the present method, the forces of the propeller are calculated locally on the inflow boundary of the disk averaged over time. As a requirement, the blade geometry (chord length distribution and blade angle) and the aerodynamic polars (lift and drag coefficient vs. angle of attack) must be given. For the investigations in this study, the propeller blade was parametrized by 50 radial stations with the corresponding data. The necessary polars were determined with the help of Xfoil in the angle of attack range of -5° to 30°. Above and below these angles of attack, a messured NACA 0012 polar was used. Based on the local inflow conditions at every cell on the front side of the disk as well as the rotational speed of the propeller, the forces in axial and tangential directions can then be calculated in each of these cells by linear interpolation of the radial stations and the provided data. Finally, the induced velocities of the propeller in the axial and circumferential directions can be calculated and imprinted on the flow field. By coupling with local flow variables, the effect of the wing on the propeller and vice versa is included, as shown in Müller et al. (2012) and Müller et al. (2014). It should be noted that this process is an iterative process that takes place while solving for the flow field. This ensures that both the effect of the propeller on the wing and vice versa are taken into account. For more information on the actuator disk model, the reader is referred to Raichle (2017), wherein a comparison with experimentally measured propeller slipstream was made. It was found, that the slipstream speeds and their distribution are very well matched. The maximum speed deviation was 4.3%. A comparison with a fully resolved propeller in front of a wing can be taken from Wales et al. (2022), wherein very good agreement between both methods was observed. The propeller designs used in the present study can be found in the section Propeller design.

Numerical Domain and Settings

The domain used for the investigations with its components is shown in figure 1. It consists of a wing with constant chord length of 1.9 m and airfoil NACA 65_2-415, a nacelle and an actuator disk modeling the propeller. The wing segment is bounded by two periodic boundaries in the spanwise direction, simulating corotating propellers. Thus, a 2.5D setup is obtained that represents a section of an infinite array of identical domains. By using this setup, spanwise effects that would occur on real wings are neglected. Thus, a transfer to a real wing geometry is outside the scope of this publication. Furthermore, support structures or pylons have not been taken into account. Preliminary studies have shown that the radius of the domain is chosen to be $250m$, which is sufficiently large that the far-field boundary condition at the outer edge does not affect the components. The coordinate system is located in the leading edge of the wing with the x axis pointing downstream. The y axis points in the spanwise direction and the z axis points upward at right angles to it. All simulations were performed at cruise flight conditions. The settings are given in the following table 1. The formation of the lift and drag coefficients which include the effect of installed propellers is shown in the following section. The data given in table 1 is representative for a future propeller-driven short-haul aircraft in cruise condition.

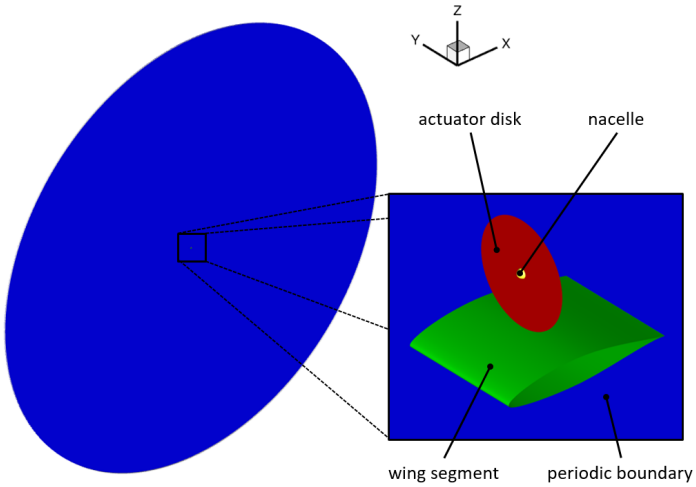

Figure 1 Numerical Domain and Components.

Table 1 Overview of settings for simulation.

Parameter	Value
Cruise speed v_∞	143 $\frac{m}{s}$
Density at cruise condition ρ_∞	0.66 $\frac{kg}{m^3}$
Pressure at cruise condition p_∞	47220 Pa
Lift coefficient at cruise condition $C_{L,glob}$	0.7146
Drag coefficient at cruise condition $C_{D,glob}$	−0.01707

Method for reaching trimmed flight condition

An iterative procedure was used to achieve the equilibrium state in cruise flight, which is shown in Figure 2. This requires global values of lift and drag coefficients in the equilibrium state $C_{L,glob}, C_{D,glob}$, as well as an initial value for the lift coefficient $C_{L,req}$, which is adjusted during iteration. The global values of the lift and drag coefficients can be obtained from Table 1 and are taken from a flight mission for a future propeller-driven short-range aircraft. The negative drag coefficient results from the inclusion of fuselage drag. Thus, in all cases, the propeller must provide more thrust than the wing segment and nacelle generate in drag. The two coefficients are defined as follows:

$$C_{L,glob} = \frac{2(F_{z,wing} + F_{z,nacelle} + F_{z,propeller})}{\rho_\infty v_\infty^2 A_{wing}} \tag{1}$$

$$C_{D,glob} = \frac{2(F_{x,wing} + F_{x,nacelle} + F_{x,propeller})}{\rho_\infty v_\infty^2 A_{wing}} \tag{2}$$

If the global coefficients and starting conditions are given, the TAU internal iteration of the angle of attack α is used to obtain the set lift coefficient. Now a secant procedure with variation of the propeller blade pitch angle follows. The results of the individual steps of the secant procedure yield the drag coefficients and the propeller thrust as well as the propeller loads in z-direction. Since the propeller in the installed condition experiences in some cases considerable nonuniform inflow conditions, it also generates loads that act in the lift direction and must be considered in the equilibrium (see equation 1). The initial value of the iteration $C_{L,req}$ is corrected for these propeller loads after each step during the procedure. Only when the coefficients of the simulation match the specifications, the case of the equilibrium state is considered to be reached. In this case, a deviation of ε is accepted, which in the present case concerned 1% of the global target value.

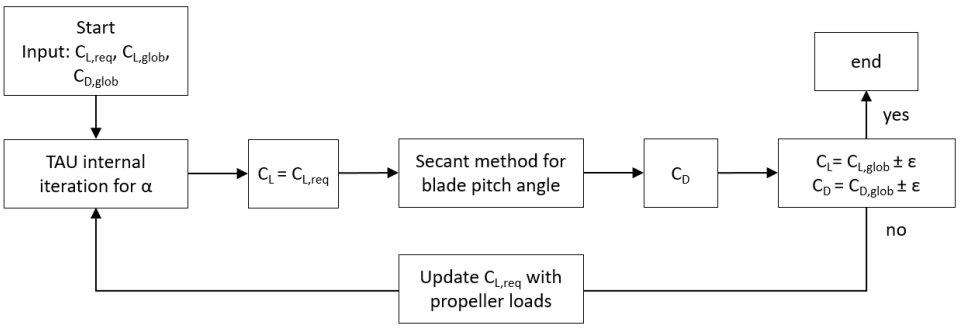

Figure 2 Method for iterating trimmed condition.

Numerical Grid

CENTAUR software from CentaurSoft (2022) was used for mesh generation. All cases were created with an unstructured mesh based on prisms and tetrahedra. Prism layers were used on viscous walls with the first layer having a dimensionless spacing of $y^+ \approx 1$. Outside the boundary layer, tetrahedra were used, refined in the region in front of and behind the actuator disk. The periodic boundaries were meshed identically to minimize numerical errors. At the beginning of the studies, a mesh convergence study was performed. For this purpose, three meshes with different resolutions were created and then evaluated using the Grid Convergence Index (GCI) according to Celik and Karatekin (1997) and Celik et al. (2008). The three calculations were performed at the center point of the DoE (see the following section). For this purpose, the medium mesh was iterated to equilibrium state using the method presented. The other two meshes were then computed with the same settings. The following figure 3 shows the influence of mesh resolution on the glide ratio of the wing as well as the power P predicted by the actuator disk. In addition, extrapolated values, shown as dashed lines, can be calculated with the method used. These are based on the Richardson extrapolation with the refinement factor of the meshes, the order of the numerical procedure and the solution of the meshes used. Based on the results, the meshing of the middle mesh with $\approx$ 36.8m cells was used and applied to the other cases.

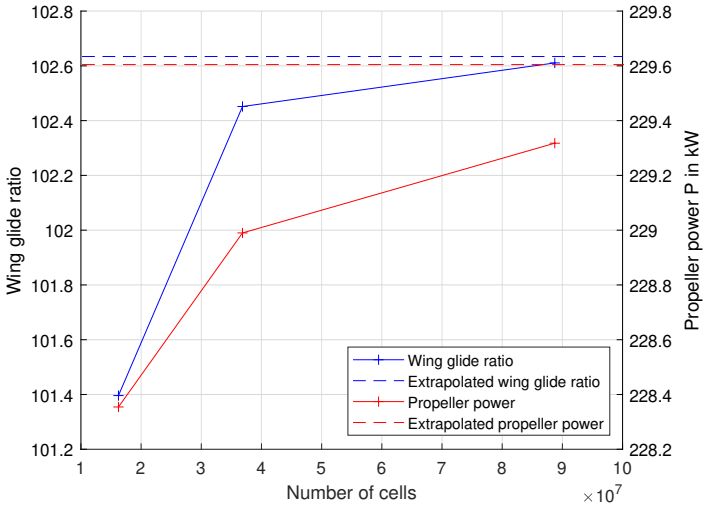

Figure 3 Results of grid convergence study.

Design of experiments (DoE)

In order to identify sensitivities of the overwing configuration, a design of experiments method was used. For this purpose, a three-level faced central composite design with five parameters was used in a first step, resulting in 43 combinations of these five parameters. The parameters with their settings are included in the following table 2. Their definition can be taken from figure 4.

Table 2 Parameters with settings for first DoE

Parameter	low level	mid level	high level
x Position (xPos)	570 *mm*	1235 *mm*	1900 *mm*
Distance to wing surface (zPos)	5 *mm*	102.5 *mm*	200 *mm*
Installation angle (InstAngle)	$-5°$	2.5°	10°
Propeller diameter (D)	1 *m*	2 *m*	3 *m*
Segment width in propeller diameter (SegWidth)	1.025	1.5125	2

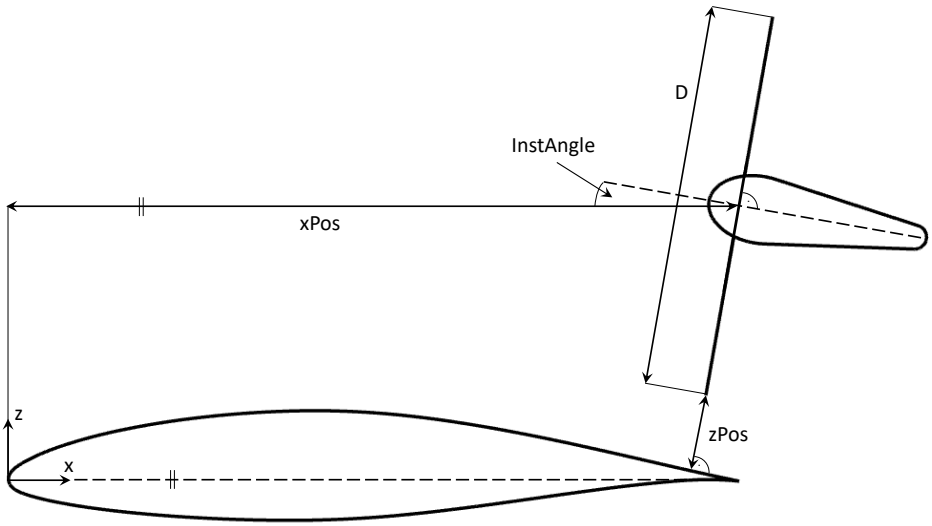

Figure 4 Parameters for DoE.

The position of the center of the actuator disk (intersection of the axis of rotation and the propeller plane) is thus defined by the x position and the distance to the upper surface of the wing. The latter is the smallest distance from the surface of the wing to the closest point of the disc. The installation angle is defined as the angle between the chord of the wing segment and the axis of rotation of the propeller. A positive value means that the propeller is rotated upwards in the positive z direction. In the present case, a normalization of the segment width (span of the segment) over the propeller diameter is appropriate, since otherwise a large number of different segment widths would have to be investigated and a three-level DoE would not be feasible.
Based on the results of the first DoE, a second DoE with reduced parameter space was then performed. For this, the position of the disk was kept constant with respect to the x position and the wing spacing. The remaining three parameters are varied in new limits, resulting in 15 more cases. The values of this second DoE are shown in the following table 3. Once the points have been calculated, a quadratic regression model can then be used to gain insight into the sensitivities in the parameter space under study.

Table 3 Parameters with settings for second DoE

Parameter	low level	mid level	high level
Installation angle (InstAngle)	0°	2.5°	5°
Propeller diameter (D)	1 *m*	1.5 *m*	2 *m*
Segment width in propeller diameter (SegWidth)	1.25	1.875	2.5
x Position (xPos)	constant 1900 *mm*		
Distance to wing surface (zPos)	constant 200 *mm*		

Propeller design

Two different propeller designs were used for the investigations. One of these designs is the widely used Xprop from TU Delft, which is used in many investigations and publications, such as Vries (2022) or Vries et al. (2021). For the investigations in this publication, the geometry of the propeller was recomputed in the tool RAPID (Lück et al. (2021)), which is based on the blade element momentum theory. Subsequently, the polars for the actuator disk were extracted.
The second propeller design (DP 2), which is additionally used in the second DoE for comparison purposes, is a design for distributed propulsion and follows the minimum induced loss design. This has been designed for lower thrust loads in the RAPID tool. Accordingly, the propeller achieves higher efficiencies with the same diameter. Characteristic values of the two propellers from the blade element momentum theory are summarized in the following table 4 for a diameter of 2 *m*. Because both propellers were calculated using the assumption of minimum induced loss with axisymmetric flow the values given in table 4 are only valid for isolated performance. When positioning the propeller over the wing the inflow field will be significantly non uniform decreasing the efficiency of the installed propeller. However, for the investigations the two propellers have been geometrically scaled. The rotational speed was determined by the requirement for a constant tip Mach number. This means that a propeller half the size must be operated at twice the rotational speed. The range of diameter was based on the number of drive units and therefore on a disk loading allowing to judge the efficiency of the isolated propeller. During scaling the hub-to-tip ratio of the propeller was kept constant at 0.16 and the nacelle was scaled

accordingly assuming that a suitable electric motor can always be designed.

Table 4 Isolated propeller performance at cruise condition

Propeller	Diameter	Rot. speed	Power	Efficiency
Xprop	2 m	1437.5 rpm	380.1 kW	0.8044
DP 2	2 m	1740 rpm	350.9 kW	0.8716

The investigations carried out in this publication focus on cruise condition to show potential benefits in this flight phase. Typically, this is not the dimensioning case for components such as the drivetrain and the propeller, which is why many investigations focus on the take-off or climb operating points with high power and thrust requirements. This is also true for the mission of the propeller-driven short-haul aircraft in this publication, for which recently the influence of the drivetrain and its sizing was investigated Keuter et al. (2023). The propellers in the present publication are designed according to the same requirements as in the cited paper.

RESULTS AND DISCUSSION

In the following the results of the DoE are shown. The power of the propellers is used as the global parameter. To make them comparable, the results are converted to a half span of the wing. For this purpose, the number of segments forming a half span of 13.46 m is determined. The following formula is used for this:

$$n_{Segment} = \frac{13.46\ m}{D\ \Delta y} \tag{3}$$

Here D is the propeller diameter and Δy is the segment width in propeller diameters. The number of segments can then be multiplied by the power of a segment $P_{Segment}$ to obtain comparable results:

$$P_{half\,span} = n_{Segment}\ P_{Segment} \tag{4}$$

Evaluation of first DoE

In the first DoE, all 5 parameters were used and calculated in 43 simulations. The investigations should give a first picture of the sensitivities. Therefore, only the Xprop was used for these investigations. The results of the simulations were used to fit a quadratic model of the form:

$$Y(x) = a + \sum_{i=1}^{N} b_i x_i + \sum_{i=1}^{N} c_i x_i^2 + \sum_{ij(i<j)} d_{ij} x_i x_j \tag{5}$$

Here a describes a constant, N is the number of calculations and x the number of parameters. b, c and d are the coefficients of the model. Thus, the model consists of linear terms (first sum of the formula 5), quadratic terms (second sum of the formula 5), and linear interactions (third sum of the formula 5). The result variable Y is the power of the halfspan as in equation 4.

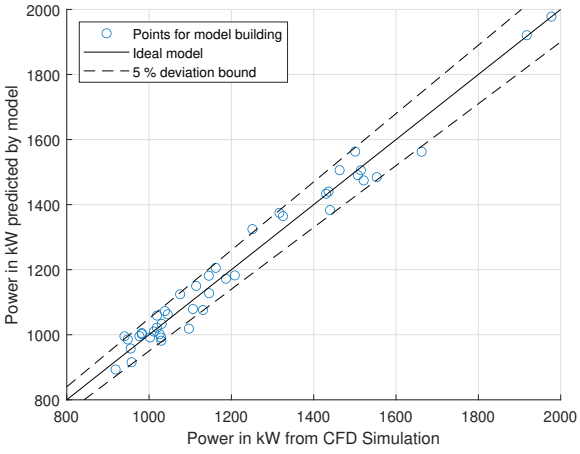

Figure 5 Power predicted by model over power resulting from simulation.

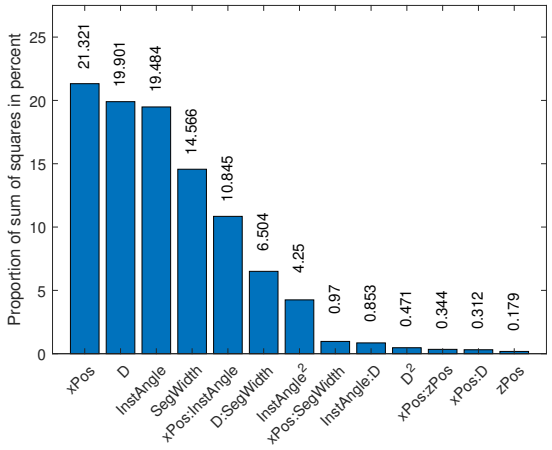

Figure 6 Contribution of parameters to sum of squares in percent.

In a first step after fitting the model with all 20 coefficients according to the previous equation, the model was reduced. This was done by using a null hypothesis for each coefficient b_i, c_i or d_{ij}. To do this, the p-value was calculated. If this was greater than 0.1, the associated coefficient was set to zero. This allowed the model to be reduced to 13 coefficients, with the coefficient of determination R^2 decreasing from 0.9799 to 0.9762. Figure 5 shows the performance predicted by the reduced model versus the performance of the simulation. From this it can be seen that with a few exceptions, the points of the model are within 5% of an ideal model. Figure 6 shows the share of the terms in the total sum of squares of the model in percent. This allows to classify how large the influence of the individual terms on the total model is. Accordingly, the response of the model can be explained by more than 95% via the first seven parameters. It is already clear here that the parameters x position, propeller diameter, installation angle and segment width have significant influences. Quadratic terms are only included for installation angle and propeller diameter and contribute comparatively little to the model. As a parameter, the distance to the top of the wing seems to be negligible. However, this will be proven later by further simulations.
First further observations and trends of the model shall be presented here. For this purpose, two parameters are contrasted in each of the following figures 7. Each combination of these parameters is evaluated at the minimum power per halfspan as in equation 4, so that only two of the five parameters are prescribed.This first stage focuses on the positioning of the propeller. Consequently, to narrow down the parameter space, the results for x position and diameter, x position and installation angle, and x position and segment width as well as segment width and diameter are shown.

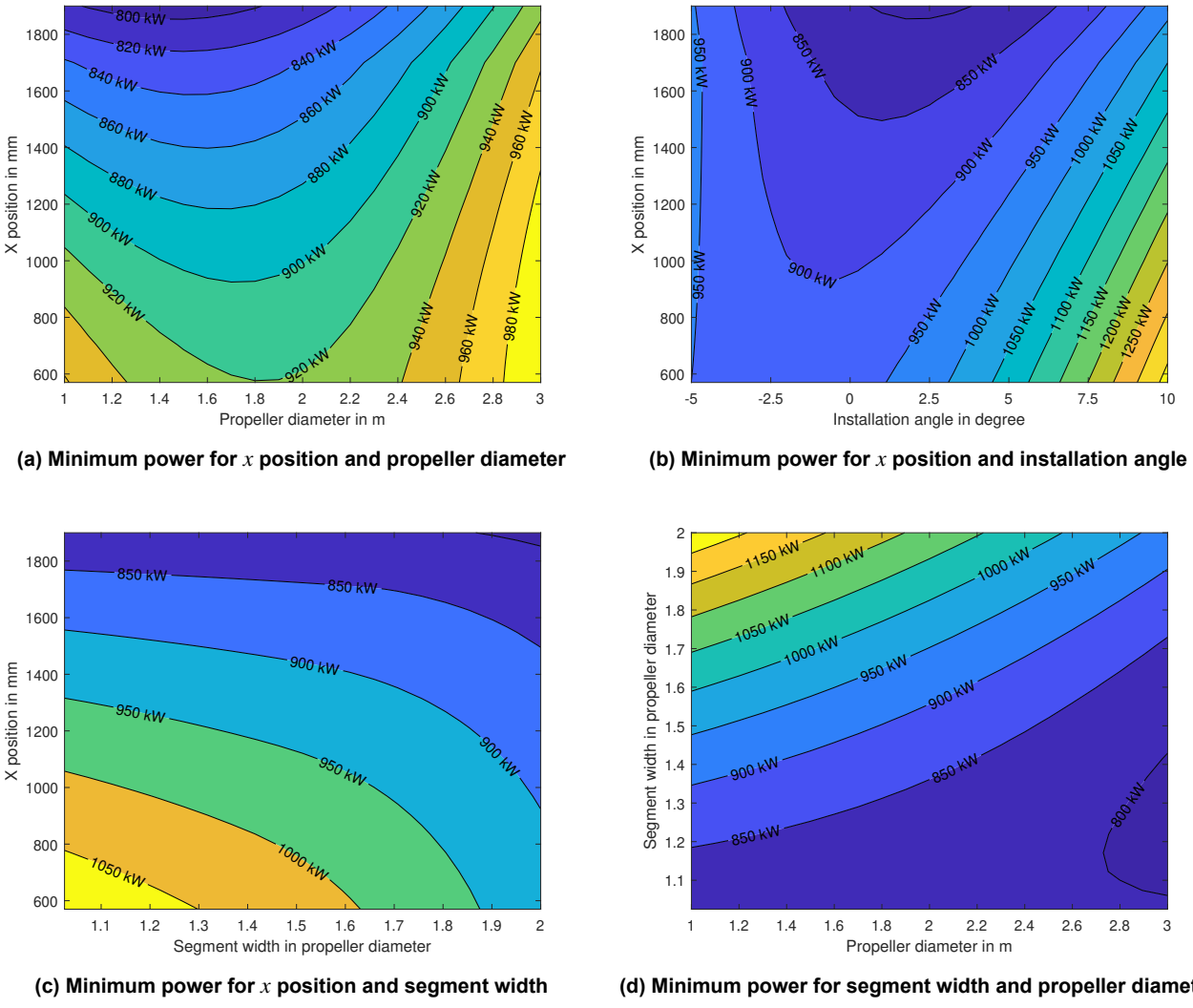

(a) Minimum power for x position and propeller diameter

(b) Minimum power for x position and installation angle

(c) Minimum power for x position and segment width

(d) Minimum power for segment width and propeller diameter

Figure 7 Minimum power for different combinations of parameters.

From the figures it can be seen that low power values always occur at far downstream x positions near the trailing edge of the wing. This is due to the velocity field at the wing. The further upstream the propeller is positioned, the greater the local velocity over the wing, so more power is required to achieve a given thrust. The interaction with the wing and the resulting drag reduction by influencing the pressure distribution of the wing, as described in Vries (2022), does not pay off

in any of the cases. Also, it is evident from figure 7a that large diameters do not provide a solution. The optimum is in the range between 1 m and 2 m diameter.
The installation angle in Figure 7b is initially notable for a fairly large flat area of power between $-2.5°$ at $x = 600$ mm and $\approx 2°$ at $x = 1900$ mm. Thus, the installation angle follows the curvature of the upper surface of the wing with some offset. However, away from this optimum, the power increases significantly. This makes the installation angle a critical parameter, since even a deviation of $1°$ outside the optimum can bring significant power increases.
Also for the segment width in figure 7c, the smallest powers occur for positions near the trailing edge of the wing. It is remarkable here, however, that the segment width has hardly any influence on the performance there. In this approximately constant region near the trailing edge between low segment widths up to 1.7, the propeller diameter remains constant at $D = 1$ m and the installation angle also remains constant, which is not shown here. This means, on the one hand, that the model reaches the limit of the parameter space there (see table 2). On the other hand, the propeller can be operated with the different thrust requirements, which are caused by a changed segment width, without large losses in efficiency. If the propeller is moved further upstream, the power increases again. However, higher segment widths seem to have advantages in this respect, since the power is lower there than with small segment widths.
In figure 7d it can bee seen that the lowest power values occur with small segment widths and large propeller diameters. However, this optimum is very flat and extends to small diameters. Since the absolute segment width (ΔyD) also increases linearly with increasing diameter, the drag of the segment also increases linearly to a good approximation. Thus, as the diameter increases, the drag increases linearly, whereas the propeller disk area ($\frac{\pi}{4}D^2$) increases quadratically. Thus, the load decreases with increasing diameter, which means that the efficiency must increase according to Froude's simple actuator disk theory. This results in lower powers for large diameters.
Not shown here are the influences of the distance to the wing, since these are very small. For a better classification of the influence of this parameter, further simulations were carried out. The following table 5 shows the influence of a variation of the distance to the wing on the performance. Thus, the distance to the wing can be classified as not significant and can be neglected. On the basis of these first investigations, a second DoE was subsequently carried out with the parameter space reduced according to table 3.

Table 5 Influence of distance to wing surface at wing trailing edge

x Position	Distance to wing surface	Installation angle	Diameter	Segment width in D	Power
1900 mm	5 mm	2.1861°	1.5 m	2	890.5 kW
1900 mm	102.5 mm	2.1861°	1.5 m	2	901.3 kW
1900 mm	200 mm	2.1861°	1.5 m	2	893.2 kW

Evaluation of second DoE

In the second DoE, the same principle as in the first DoE was used. The parameter space was reduced to three parameters. The propeller was always positioned above the trailing edge of the wing at a fixed distance. Only the diameter, segment width and installation angle were varied within the limits shown in Table 3. In addition, a second propeller (DP 2) with higher efficiency was calculated for the same conditions for comparison purposes.

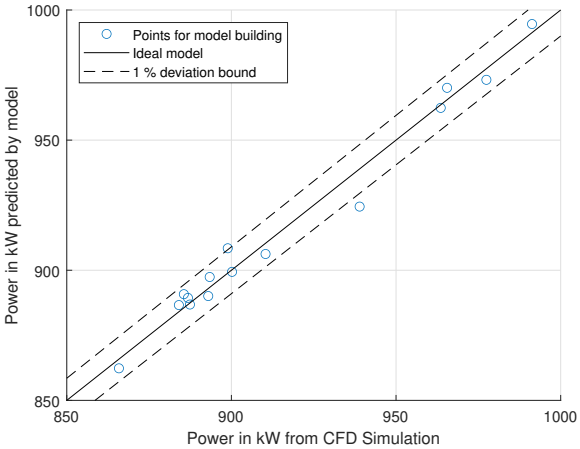

Figure 8 Power predicted by model over power resulting from simulation in second DoE for Xprop.

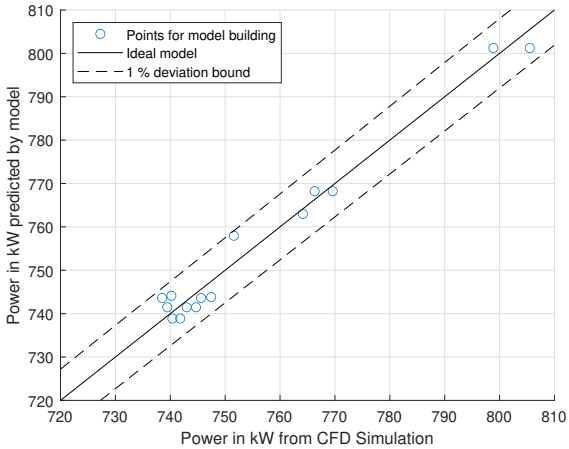

Figure 9 Power predicted by model over power resulting from simulation in second DoE for DP2.

The results are shown here for both propeller designs simultaneously. In both cases, after the simulations, a quadratic model as in equation 5 has been fitted to the data by regression. As in the first step, a reduction in the number of model coefficients from nine to seven in the case of the Xprop and five in the case of the DP2 was performed. In doing so, the coefficient of determination R^2 decreased slightly from 0.9833 to 0.98 when using the Xprop and from 0.9827 to 0.9755 for the DP 2 propeller. Figures 8 and 9 show the comparison of model and simulation. In the case of the Xprop, two of the 15 points are just outside the 1% limit. In the case of the DP2 propeller, all points are within this limit.

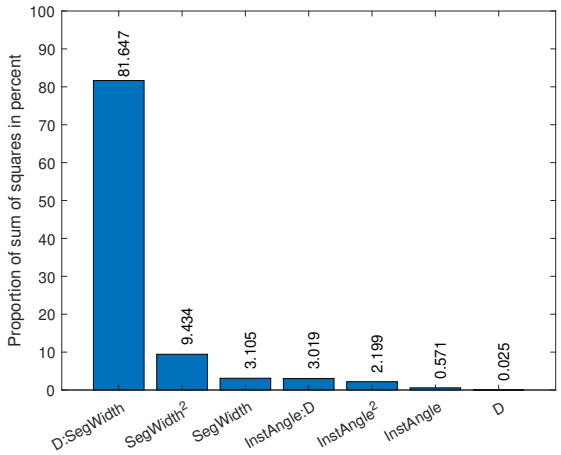

Figure 10 Contribution of parameters to sum of squares in percent in second DoE for Xprop.

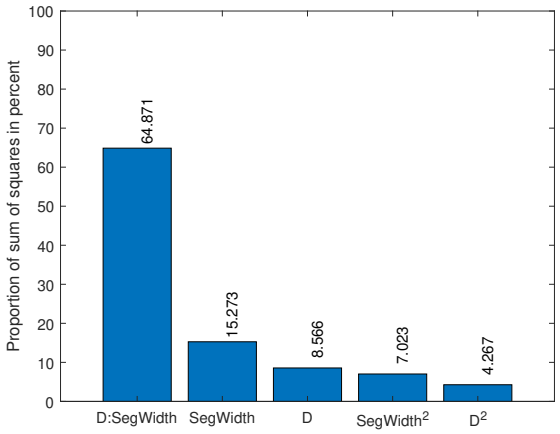

Figure 11 Contribution of parameters to sum of squares in percent in second DoE for DP2.

In the figures 10 and 11 the proportions of the terms in the sum of squares are shown. Here it is shown that in both cases the linear interaction of segment width and diameter has a decisive influence. Furthermore, the segment width as a parameter together with the interaction of the diameter stands for about 94% of the model response in the model of the Xprop and for 87% in the model of the DP2 propeller. The installation angle plays a minor role in both models. This has even disappeared completely from the model in case the DP2 propeller is used. Thus, the models are evaluated at different diameters and segment widths, as shown in the following figures 12 and 13.

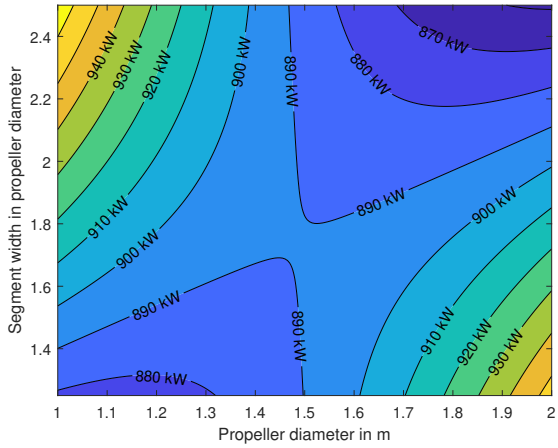

Figure 12 Minimum power for segment width and propeller diameter for Xprop.

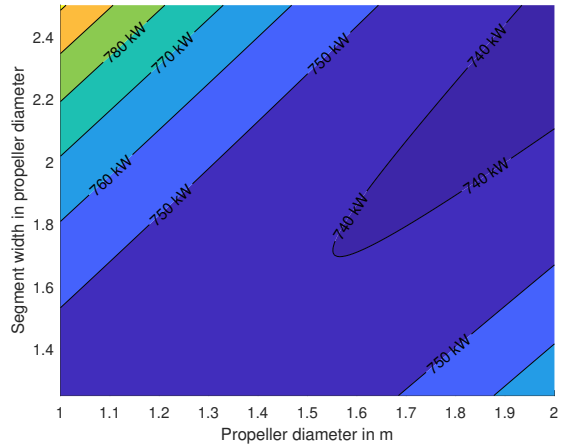

Figure 13 Minimum power for segment width and propeller diameter for DP2.

In both figures, a flat channel-like area can be seen running diagonally across the area from bottom left to top right. This area indicates the optimum between propeller diameter and segment width and thus the distribution of the drives on the wing. By comparing the figures it can be seen that this area is somewhat steeper in the case of the Xprop than in the case of the DP2 propeller. In general, however, these figures are similar in their characteristics. Only the absolute values of the power are lower when using DP2 propeller due to the higher efficiency of this propeller. However, both figures have their optimum near the right edge at large diameters ($D = 2\ m$) and high segment widths (≈ 2.5). Converted to a half span of 13.46 m with equation 3 this would mean only about three propellers per half span. However, the figures also show that

a small deviation from the optimum does not cause any major disadvantages. Thus, the optimum depends on the ratio of diameter to segment width. This means, however, that as soon as one of the parameters diameter or segment width is set, the other parameter is also fixed accordingly. This applies almost independently of the propeller used.

CONCLUSION

In this paper, sensitivities of distributed propeller propulsion in overwing configuration at cruise conditions were investigated using a DoE. For this purpose, a setup consisting of a wing segment with constant chord length, an actuator disk modeling the propeller, and a nacelle was used. All calculations were brought to an equilibrium state using an iterative procedure so that the propeller power can be used as the evaluation parameter. The DoE was performed in two stages. In the first DoE, it was found that for a x position near the trailing edge of the wing, the lowest powers are required for the overall system. In this case, the distance of the propeller from the top of the wing is not significant in the limits studied. Consequently, in the second DoE, the propeller was positioned above the trailing edge of the wing with a constant distance to the top surface to gain further insight into the distribution of the propellers, their size as well as installation angles. It was found that the segment width or the distance between the propellers has a significant influence. The strong interaction with the propeller diameter results in an optimal segment width for each propeller diameter. The performance of the overall system is approximately constant along this combination. This was also observed in studies with a second propeller with higher efficiency. The values for power were reduced as expected, but show a very similar pattern. Future studies will address the transfer of the results to 3D wings. This will also have to include the issue of necessary support structures and pylons in overwing configurations and their effect on the results presented here. Both simplifications (missing 3D wing effects and pylons) are expected to have an impact on the results shown in this publication increasing power.

NOMENCLATURE

a	Constant in regression model
A	Area
b	Coefficient of regression model
c	Coefficient of regression model
C_D	Coefficient of Drag
C_L	Coefficient of Lift
d	Coefficient of regression model
D	Propeller diameter
F	Force
N	Number of parameters in regression model
p	Static pressure
P	Propeller power
v	Speed
x	Parameter in regression model

Greek symbols

α	Angle of attack
Δy	Segment width in propeller diameter
ε	Deviation
ρ	Density

Superscripts and subscripts

$glob$	Global value for trimmed condition
$halfspan$	Value referred to half of the span
$nacelle$	Value referred to nacelle
$propeller$	Value referred to propeller
req	Value during iteration of trimmed condition
$segment$	Value referred to one segment
$wing$	Value referred to wing
x, y, z	Direction of coordinate system
∞	Free stream value

Abbreviations

DoE	Design of experiment
DP2	Propeller used for investigations
RAPID	Research Algorithm for Propeller Identification and Design
Xprop	Propeller used for investigations

ACKNOWLEDGMENTS

The authors would like to acknowledge the funding by the Deutsche Forschungsgemeinschaft (DFG, German Research Foundation) under Germany's Excellence Strategy – EXC 2163/1 - Sustainable and Energy Efficient Aviation – Project-ID 390881007. Furthermore the work was supported by the North-German Supercomputing Alliance (HLRN).
The authors would like to thank Dr. Tomas Sinnige from TU Delft for his valuable advice and fruitful discussions.

References

Beckers, M. F., Schollenberger, M., Lutz, T., Bongen, D., Radespiel, R., Florenciano, J. L. and Funes-Sebastian, D. E. (2023), 'Numerical Investigation of High-Lift Propeller Positions for a Distributed Propulsion System', *Journal of Aircraft* .

Bernardini, G., Centracchio, F., Gennaretti, M., Iemma, U., Pasquali, C., Poggi, C., Rossetti, M. and Serafini, J. (2020), 'Numerical Characterisation of the Aeroacoustic Signature of Propeller Arrays for Distributed Electric Propulsion', *Applied Sciences* **10**(8).

Celik, I., Ghia, U., Roache, P. J. and Freitas, C. J. (2008), 'Procedure for Estimation and Reporting of Uncertainty Due to Discretization in CFD Applications', *Journal of Fluids Engineering* **130**(7).

Celik, I. and Karatekin, O. (1997), 'Numerical Experiments on Application of Richardson Extrapolation With Nonuniform Grids', *Journal of Fluids Engineering* **119**(3), 584–590.

CentaurSoft (2022), 'Centaur hybrid grid generation system'. [Online; accessed 10th November 2022].
URL: *https://www.centaursoft.com*

Cooper, R. K., McCann, W. J. and Chapleo, A. Q. (1992), Over wing propeller aerodynamics, *in* 'ICAS Proceedings (AIAA)'.

Deere, K. A., Viken, J. K., Viken, S., Carter, M. B., Wiese, M. and Farr, N. (2017), Computational Analysis of a Wing Designed for the X-57 Distributed Electric Propulsion Aircraft, *in* '35th AIAA Applied Aerodynamics Conference'.

Della Vecchia, P., Malgieri, D., Nicolosi, F. and De Marco, A. (2018), 'Numerical analysis of propeller effects on wing aerodynamic: tip mounted and distributed propulsion', *Transportation Research Procedia* **29**.

Giraldo, D. A., Roger, M., Jacob, M. C. and Beriot, H. (2022), Analytical study of the aerodynamic noise emitted by distributed electric propulsion systems, *in* 'AIAA/CEAS Aeroacoustics 2022 Conference'.

Johnson, J. J. and White, E. (1983), Exploratory low-speed wind-tunnel investigation of advanced commuter configurations including an over-the-wing propeller design, *in* 'AIAA Aircraft Design, Systems and Technology Meeting'.

Keller, D. (2021), 'Towards higher aerodynamic efficiency of propeller-driven aircraft with distributed propulsion', *CEAS Aeronautical Journal* **12**(4), 777–791.

Keuter, R. J., Kirsch, B., Friedrichs, J. and Ponick, B. (2023), 'Design Decisions for a Powertrain Combination of Electric Motor and Propeller for an Electric Aircraft', *IEEE Access* .

Kirsch, B. and Friedrichs, J. (2023), CFD Parameter Studies using an Actuator Disk to Quantify the Interactions on an Airfoil Segment for Distributed Propulsion, *in* 'Proceedings of the ASME 2023 Turbomachinery Technical Conference and Exposition'.

Lück, S., Göing, J., Wittmann, T., Kirsch, B., Benjamin, L. and Friedrichs, J. (2021), Propeller Design and Performance Evaluation with Partially Prescribed Velocity Distribution, *in* 'Proceedings of Global Power and Propulsion Society'.

Menter, F., Kuntz, M., Langtry, R., Hanjalic, K., Nagano, Y. and Tummers, M. J. (2003), 'Ten Years of Industrial Experience with the SST Turbulence Model', *Turbulence, heat and mass transfer* **4**, 625–632.

Müller, L., Kozulovic, D., Hepperle, M. and Radespiel, R. (2012), Installation Effects of a Propeller Over a Wing with Internally Blown Flap, *in* '30th AIAA Applied Aerodynamics Conference'.

Müller, L., Kozulovic, D. and Radespiel, R. (2014), 'Aerodynamic Performance of an Over-the-wing Propeller Configuration at increasing Mach number', *CEAS Aeronautical Journal* **5**(3), 305–317.

Raichle, A. (2017), Flusskonservative Diskretisierung des Wirkscheibenmodells als Unstetigkeitsfläche, PhD thesis, DLR - Institute of Aerodynamics and Flow Technology, Braunschweig, Germany.
URL: *https://elib.dlr.de/125185/*

Raichle, A., Melber-Wilkending, S. and Himisch, J. (2008), A New Actuator Disk Model for the TAU Code and Application to a Sailplaine with a Folding Engine, *in* C. Tropea, S. Jakirlic, H.-J. Heinemann, R. Henke and H. Hönlinger, eds, 'New Results in Numerical and Experimental Fluid Mechanics VI', Springer Berlin Heidelberg, Berlin, Heidelberg, pp. 52–61.

Schwamborn, D., Gerhold, T. and Heinrich, R. (2006), 'The DLR TAU-Code: Recent applications in research and industry', *ECCOMAS CFD 2006 CONFERENCE* .
URL: *https://elib.dlr.de/22421/*

Spinner, S., Keller, D., Schnell, R. and Trost, M. (2020), A Blade Element Theory Based Actuator Disk Methodology for Modeling of Fan Engines in RANS Simulations, *in* 'AIAA Aviation Forum'.

Veldhuis, L. L. M. (2005), Propeller Wing Aerodynamic Interference, PhD thesis, TU Delft, Delft, Netherlands.
URL: *http://resolver.tudelft.nl/uuid:8ffbde9c-b483-40de-90e0-97095202fbe3*

Vries, R. d. (2022), Hybrid-Electric Aircraft with Over-the-Wing Distributed Propulsion: Aerodynamic Performance and Conceptual Design, PhD thesis, TU Delft.

Vries, R. d., van Arnhem, N., Sinnige, T., Vos, R. and Veldhuis, L. L. M. (2021), 'Aerodynamic interaction between propellers of a distributed-propulsion system in forward flight', *Aerospace Science and Technology* **118**.

Wales, C., Jones, D., Gaitonde, A., Risley-Settle, P. and Peace, A. (2022), Comparison of Aircraft Loads Using URANS and Actuator Disk Modelling of Propellers, *in* 'AIAA Aviation Forum'.